International Journal of ISSI, Vol.11 (2014), No.1, pp.1-6

The Effect of Inclusions on Through-thickness Directional Fatigue Behavior of S355N Steel Plate

A. Abyazi[1] , A. R. Ebrahimi[2]*
[1]Faculty of Materials Engineering, Sahand University of Technology, Tabriz, 5331711111, Iran
[2] Department of Mining and Metallurgical Engineering, Amirkabir University of Technology, Tehran, 158754413, Iran

Abstract

Microalloyed S355N steel plates are extensively used in bridge and high-rise building structures. One of the factors affecting the mechanical properties is the size and morphology of inclusions. In this research, microalloyed S355N steel plates with different sizes of inclusions were examined. One contained long manganese sulfide inclusions (LI material) and the other had short ones (SI material). Fatigue and tensile tests were carried out in through-thickness direction of both materials. Additionally, the fatigue test results were verified by "statistics of extreme value" (SEV) method. The tensile and fatigue tests revealed that toughness and fatigue limit of LI material were 65% and 30% less than those of SI, respectively. The SEV analysis conservatively predicted the fatigue limit of SI material. However, it was not accurate enough in the case of LI. These results could be explained using the behavior of manganese sulfide inclusions as short fatigue cracks in steels.

Keywords: Fatigue, Through-thickness direction, Non-metallic inclusion, Short fatigue crack, Statistics of extreme value.

1. Introduction

Microalloyed steels are extensively used in making large structures such as ships, bridges and high buildings [1-3]. Most of these steels are made by hot rolling process. The heterogeneous nature of the hot deformation process causes the anisotropy of steel plates [4-9]. The degree of anisotropy depends on rolling condition as well as the purity and the composition of steel [4,7]. Parameters such as type, shape, size and distribution of inclusions in steel plate have a major effect on the anisotropy of mechanical properties [10-13]. There are many studies and standards in the field of quality control of steels regarding the type, size and other characteristics of inclusions [14-18]. Murakami et al. carried out extensive researches regarding the effect of inclusions on the fatigue behavior of steels [19-23] and introduced the statistics of extreme value (SEV) method. This technique was developed to characterize the features of inclusions in steel by the combination of image and statistical analyses [17, 20, 22, 23]. It could also predict the fatigue limit of steel structures [22]. Some researchers have mentioned the efficiency of SEV method in the case of various steels [24-27]. One objective of this study was the application of SEV method to S355N steel.

S355N, as a fine-grain and microalloyed steel plate, is widely used in steel bridges in Europe, the United states of America and Iran [28]. Previous studies on the tensile anisotropy of S355N steel [29] have shown that its mechanical properties are strongly dependent on plate direction. In the continuation of previous research [28-31], two types of S355N steel were used in the present study. Both types contained manganese sulfide inclusions in which one had long inclusions and the other had short ones. The effect of inclusions on through-thickness directional fatigue behavior of both S355N steels was evaluated. By applying the SEV to both steels, their fatigue limit was predicted. Then, the accuracy and reliability of SEV in evaluating the through-thickness fatigue limit of both steels were assessed.

2. Materials and Methods

The chemical compositions of SI and LI materials with 40 mm thickness as well as the standard values are presented in Table 1.

**Corresponding author*
Tel: +98 411 3444334
Email: a.abyazi@gmail.com
Address: Faculty of Material Engineering, Sahand University of Technology, Tabriz, Iran
1. Ph.D. Student
2. Associate Professor

Table 1. Chemical composition of LI and SI materials (in wt%).

Element	C	Si	Mn	P	S	Ti	Nb	V
SI material	0.15	0.32	1.36	0.023	0.007	0.004	<0.002	0.003
LI material	0.17	0.23	1.44	0.017	0.009	0.004	<0.002	0.003
DIN 10113	0.20	0.50	1.65	0.030	0.025	0.030	0.050	0.120

After polishing the metallographic specimens with emery papers, their surfaces were mirror-finished to 1μm by alumina powder. The metallographic specimens were etched with 2% nital. Microstructural images of specimens were prepared using an optical microscope model MPG3. The characteristics of inclusions were described by image analysis software. The through-thickness tensile and fatigue specimens were prepared according to the procedure brought in the reference [28]. The tensile and fatigue specimens were prepared according to ASTM/A770 and DIN50113, respectively. After machining, the fatigue specimens were ground and polished carefully with SiC paper up to 1200 grade to ensure that all machining marks be removed from the specimens. Fatigue tests with hourglass shaped specimens (Fig. 1) having a gauge diameter of 5 mm were conducted on a rotary bending fatigue test machine (model: Roell Amsler UBM 200) at 3000 rpm.

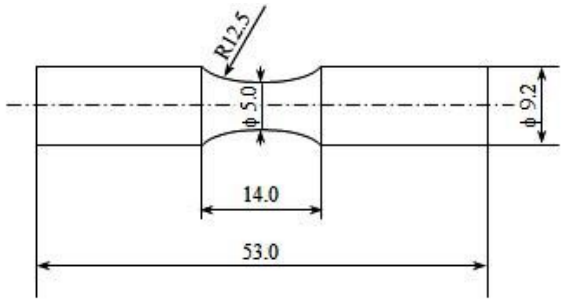

Fig. 1. The shape of fatigue test specimen (dimension in mm).

All tests were done with the stress ratio of R= −1 in the laboratory and at the ambient temperature. Tensile tests were performed at room temperature on an Instron 8502 hydraulic machine using a strain-gage extensometer for the strain measurement of specimens. Tensile test specimens were strained at the across-head speed of 2 mm per minute. The fractography studies were carried out using a MV 2300 Cam Scan field -emission scanning electron microscopy (SEM). To predict the largest inclusion size as well as the fatigue limit of LI and SI materials, the SEV method was used according to the reference [20, 22].

3. Results and Discussion

3.1. Microstructure

Fig.2 shows the microstructure of LI and SI materials. This kind of banded microstructure (Fig. 2a) is common in hot-rolled steel plates [32-34]. According to Fig. 2a, the dark phase was pearlite and the gray phase was ferrite under optical microscopy. Fig. 2a-1 shows the elongated manganese sulfide inclusions beside the pearlite layer in LI material.

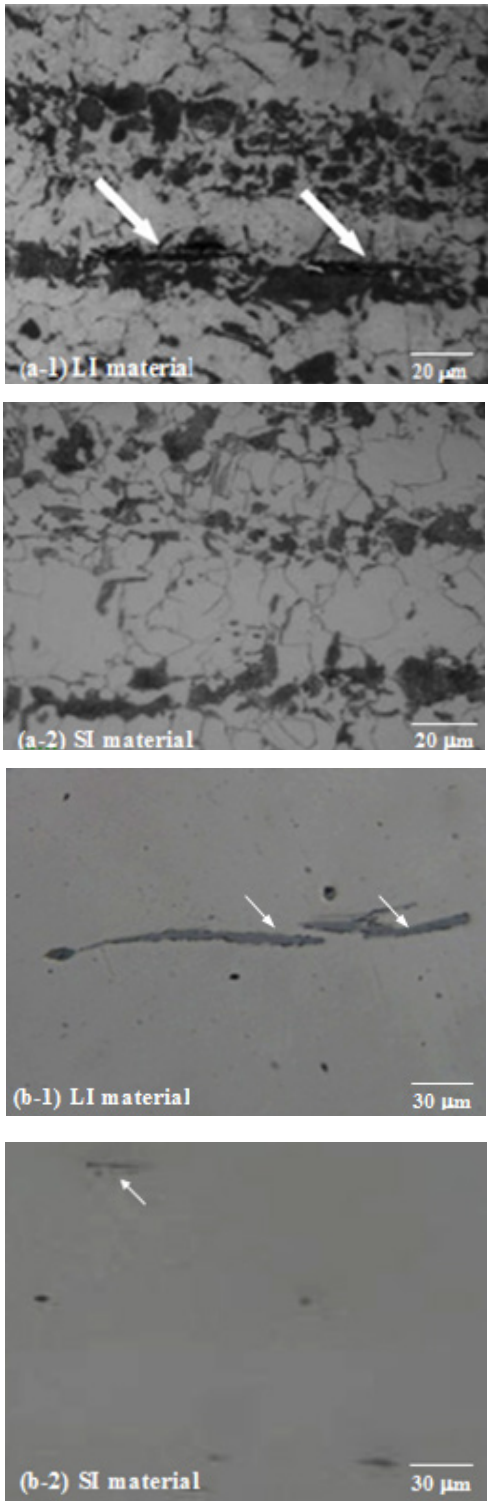

Fig. 2 The microstructure of LI and SI materials, (a) The etched microstructures, (b) The un-etched microstructures, the arrow shows the MnS inclusions

3.2. Inclusions characteristics

Fig.2b shows the non-metallic inclusions of both LI and SI materials in the un-etched condition. The average size of these manganese sulfide inclusions in LI and SI materials was 21.0 and 12.4 μm and the aspect ratio was 12 and 3, respectively.

The results of statistics related to extreme distributions of both materials are shown in Fig. 3. By considering the graph of Fig. 3, the largest possible size of inclusion in fatigue specimens of LI and SI materials was predicted as follows [22].

$\sqrt{area}_{max} = 8.130\, y_j + 16.748 \longrightarrow \sqrt{area}_{max} = 76.9\,\mu m \approx 77\mu m$ LI material

$\sqrt{area}_{max} = 3.984\, y_j + 10.279 \longrightarrow \sqrt{area}_{max} = 41.8\,\mu m \approx 42\mu m$ SI material

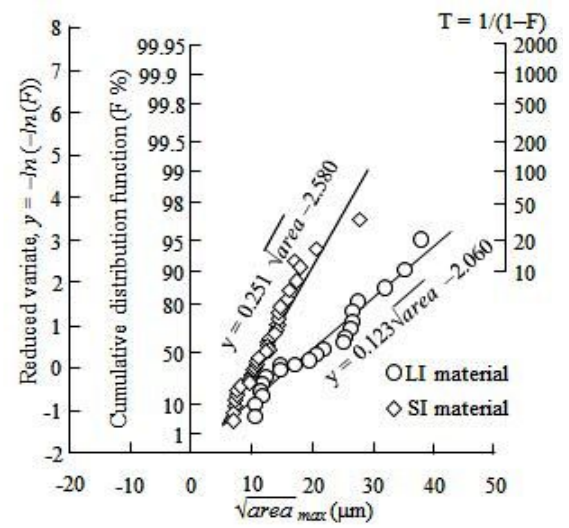

Fig. 3. Statistics of extreme value distribution of inclusions in LI and SI materials.

3.3. Tensile properties

Typical strain-stress curves as well as the results of tensile tests are shown in Fig. 4 and Table 2, respectively. The ultimate tensile strength of SI material was approximately 60 MPa more than that of LI material. Table 2 reveals that the fracture strain and reduction in the area of SI material were 3.2 and 2.9 times more than those of LI, respectively.

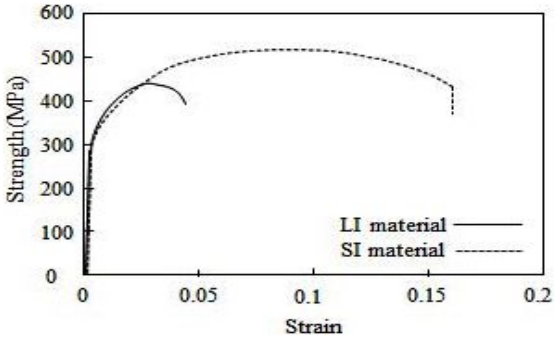

Fig. 4. The stress-strain curves of LI and SI materials.

Table 2. The results of tensile tests of LI and SI materials.

Material	RA[1] (%)	ε_f[2] (%)	σ_{UTS}[3] (MPa)
LI	18	4.6	444
SI	52	14.9	505

1 Redaction in area
2 Nominal fracture strain
3 Ultimate tensile strength

Fig.5 shows the fracture surface of tensile specimens. Fig.5a-1 also shows a rough fracture surface of LI material. The higher magnification of point * from Fig. 5a-1 is shown in Fig. 5b-1. It revealed many elongated manganese sulfide inclusions in the tensile fracture surface of the LI material, which had a detrimental effect on the plastic deformation of LI material. Fig. 5a-2, however, shows that fracture surface of SI material was not rough. According to Fig. 5b-2, there were many fine dimples all over the surface, indicating the ductile fracture of SI material.

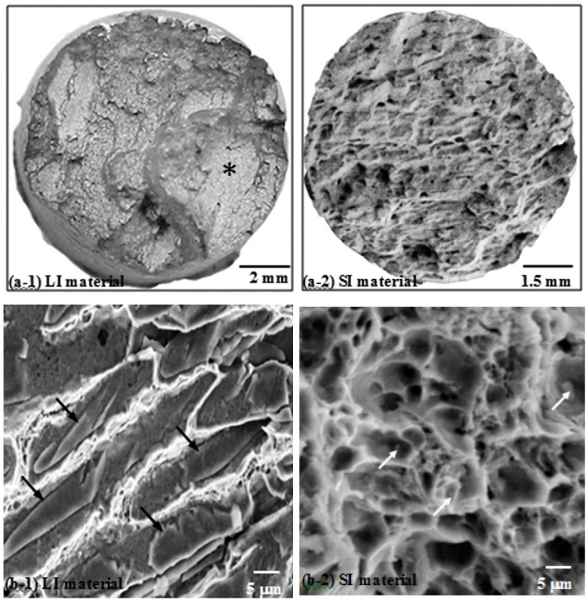

Fig. 5. SEM images of tensile fracture surfaces for the (a) overall fracture surface and (b) higher magnification of LI and SI materials.

The stepwise and rough nature of the fracture surface of tensile test specimens could be due to the "shear junction phenomenon" [35]. In LI material, the shear junction between the nucleated cracks of different surfaces in crack growth process caused the rough and stepwise fracture surface (Fig. 5a-1). It has been reported that shear junction is due to the necking between inclusions or the shear stress concentration between the separated inclusion and the matrix [36].

3.4. Fatigue properties

Fig.6 illustrates the S-N diagram of both SI and LI materials and shows the fatigue limit of290 MPa and 160 MPa, respectively. Considering the close chemical

compositions of the two materials, it could be deduced that long inclusions in LI material facilitated the fatigue crack initiation and/or propagation compared with the SI material. The fatigue limit of LI material had a significant reduction (about 45%) due to the existence of manganese sulfide inclusions with a maximum size of ≈77μm compared to the SI material. Murakami et al. [25] studied the fatigue behavior of specimens containing artificial defects of different sizes in the low carbon and medium-carbon steels. They pointed out that inclusions longer than a critical size had a significant effect on the fatigue behavior. They reported that the critical size in low-carbon steel (0.13% C) was about 70 μm and in medium-carbon steel (0.46% C) about 35μm. By comparing the carbon content of S355N steel (0.16%) with that of Murakami's work, one could find that the critical crack length of S355N steel was slightly less than 70 μm. It was assumed that manganese sulfide inclusions in SI material with a maximum length of 42 μm and in LI material with a maximum length of 77 μm were considered as short fatigue cracks[1] . In this case, it could be concluded that the crack size in SI material was less than the critical crack length of S355N steel.

However, in LI material, due to the existence of larger crack size in comparison to the critical crack length of S355N steel, the fatigue limit was reduced significantly.

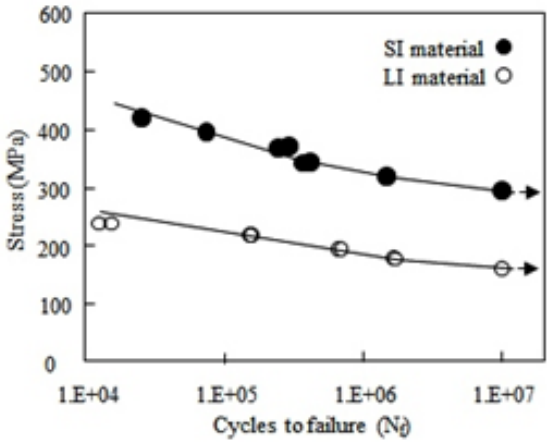

Fig. 6. The fatigue behavior of LI and SI materials.

The fatigue fracture surface of both materials is shown in Fig. 7, illustrating a typical striation pattern in the SI material (Fig. 7a-2). It contained three distinct areas including crack nucleation (zone 1), crack propagation (zone 2) and the final fracture (zone 3). However, the fatigue fracture surface of LI material displayed a different appearance (Fig. 7a-1). It contained extensive stepwise areas that could have arisen from multiple fatigue crack nucleation locations as well as competitive fatigue crack growth. Fig.7b depicts the fatigue crack growth area of both materials. It shows that the crack growth path in the SI material (Fig. 7b 2) was smooth, as compared with that of LI material (Fig. 7b 1), which was rough. According to Fig. 7b 1, there was a crack below the surface which could be considered as secondary crack. The fatigue crack tip stress field could cause the opening of the weak manganese sulfide interface in the presence of long inclusions. This led to the formation of secondary fatigue cracks that grew together with the primary ones. This phenomenon could lead to the fracture surface roughness. Similar observations were reported by Temmel et al. [37] .

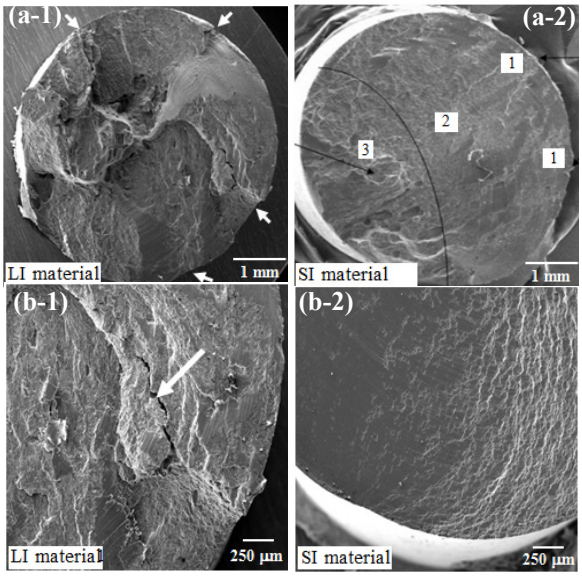

Fig. 7. SEM images of fatigue fracture surfaces for the (a) overall fracture surface and (b) higher magnification of LI and SI materials.

Fig.8 shows the elongated manganese sulfide inclusions in the fatigue crack nucleation area of LI material. These elongated inclusions were aggregated adjacent each other as the stringers. Here, the size and aspect ratio of each inclusion were at least 40 μm and 20, respectively. No inclusion was found in the fatigue crack nucleation area of the SI material. The nucleation of fatigue crack from inclusions in LI material happened due to the large inclusion size, their close distance and the weak interface between large manganese sulfide inclusions and the matrix [37,38].

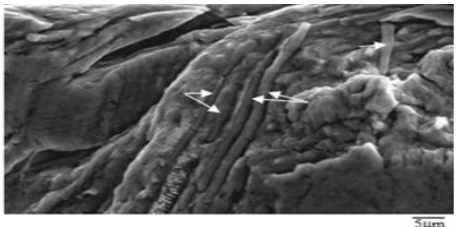

Fig. 8. The nucleation of fatigue crack from inclusions in LI materials. Arrows show the elongated manganese sulfide inclusions.

[1] *The short crack behavior is observed at crack dimensions which are about equal to the micro-structural dimensions of the material or the plastic zone.*

The aspect ratio of inclusions in fatigue crack nucleation area of LI material (20) was greater than that obtained from metallographic investigations [12]. This was probably due to the orientation of the metallographic sample. The inclusion length measurements in metallographic specimens were significantly dependent on the specimen axis on which the polishing plane had to be parallel to the hot-working axis. If the polishing plane were deviated more than 6 degrees [18] from the longitudinal hot-working axis in the case of long inclusions, the results would not have been sufficiently accurate.

The less fatigue limit of LI material, in comparison to that of the SI one, could be explained using the behavior of manganese sulfide inclusions as short fatigue cracks. Different microstructural regions such as grain boundaries and secondary phases [39-41], as well as the banded steels in the ferrite-perlite interface, the ferrite-ferrite grain boundary, ferrite grain body and inclusion-matrix interface [42], can act as the short fatigue crack initiation sites. Naraisah et al. [43] carried out research on the mechanism of short crack nucleation in several steels. In the case of banded SA333 steel with short inclusions, they recognized that the short cracks (average size: 8.6±3.4 μm) were nucleated from the ferrite perlite interface. They also stated that in SA333 steel, short cracks could not be nucleated from inclusions. Similarly, in the SI material, the inclusions did not play any essential role in nucleation and/or propagation of short fatigue cracks. Other locations such as ferrite-pearlite interface could act as fatigue crack nucleation sites. However, in the case of LI material, the manganese sulfide inclusions were the preferred region for short fatigue crack nucleation and/or propagation. As a result, the short fatigue cracks in LI material were longer than those of the SI material. It has been well established that rapid crack propagation occurs in longer short cracks [44]. Thus, it is expected that the fatigue limit of LI material be less than the SI material.

3.5. The predicted fatigue limit (the SEV method)

As explained in the previous section, the fatigue fracture origin of LI material was from elongated inclusions below the specimen surface. In the case of the SI material, no inclusion was observed in fatigue crack nucleation sites. In this case, by considering the hardness of steels as 154.5kgf/mm^2, the fatigue limit of SI and LI materials was predicted to be 209 MPa and 189 MPa, respectively. The fatigue limit of SI and LI materials was, respectively, 81 MPa and 29 MPa more and less than that of the predicted results.
Similar to the findings of other researchers [17, 22], the prediction of fatigue limit in SI material was conservative. However, the predicted fatigue limit of LI material was more than the experimental fatigue limit. Similar trends have been observed in the literature [45].

The SEV investigation of Kanbe et al. [45] on the manganese sulfide inclusions of 17CrMo4 steel showed that in the case of long inclusions with a high aspect ratio, the SEV method was not conservative. They indicated that in the case of elongated inclusions, sufficient accuracy in SEV method could be achieved when the polishing plane was parallel to hot-working direction. Hence in this case, the polishing plane should not be deviated more than 1 degree from the hot-working axis [45]. It can be deduced that in the case of steels with long inclusions, the SEV method cannot be applied with sufficient conservatism since inclusions may not be perfectly parallel to the rolling direction.

4. Conclusions

1- In S355N steels containing inclusions with the maximum size of 42 and 77 μm, the fatigue limit was 290 MPa and 160 MPa, respectively.
2- Through-thickness directional fatigue limit of steel containing long manganese sulfide inclusions was 45% less than that of steel containing short manganese sulfide.
3- Manganese sulfide inclusions were observed in the fatigue fracture surface of S355N steel containing long inclusions. However, in the fracture surface of S355N steel with short inclusions, there were no observable inclusions.
4- The fracture strain and reduction of area in through-thickness direction of steel with short manganese sulfide inclusions were 3.2 and 2.9 times more than those of S355N steel with long manganese sulfide inclusions.
5- In the case of steel with long manganese sulfide inclusions, the statistics of extreme value were not accurate enough.

References

[1] G. Owens, A. Wood: J. Construct. Steel Res., 46(1998), 32.
[2] T. Kitada, J. Construct: Steel Res., 62 (2006), 1192.
[3] M. C. Moynihan, J. M. Allwood: Resour. Conser. Recycl., 68(2012), 88.
[4] J. Heuschkel: Weld. J., (1971), 110-s.
[5] A. Streisselberger, V. Schwinn, R. Hubo: Proc. of the Int. Symp. Niobium, Miner. Met. Mater. Soc., Orlando, FL, United states, (2001).
[6] J. I. Verdeja, J. Asensio, J. A. Pero-Sanz: Mater. Charact., 50(2003), 81. [7] I. C. Mayes, T. J. Baker: Mater. Sc. Tech., 2(1986), 133.
[8] T. Suzuki, Y. Tomota, M. Isaka, A. Morial, N. Minakawa, Y. Morii: ISIJ Int., 44(2004), 1426.
[9] S. Hirose, N. Rattanasuwannachart, C. Miki: Proc. of 2nd Int. conf. on Structural stability and dynamics, Singapore, (2003), 134.
[10] D. Daniel, J.J. Jonas: Metall. Trans. A, 21A(1990),

[11] A. Mateo, L. Lianes, N. Akdut, J. Stolarz, M. Anglada: Int. J. Fatigue, 25(2003), 481.
[12] W. A. Spitzig: Metall. Trans. A, 14A(1983), 271.
[13] A. Ray, S. K. Paul, S. Jha: J. Mat. Eng. and Perform. 4(1995), 679.
[14] G.R. Speich, W. A. Spitzig: Metall. Trans. A, 13A(1982), 2239.
[15] S. K. Dhua, A. Ray, S. K. Sen, M. S. Prasad, K. B. Mishra, S. Jha: J. Mater. Eng. Perform. 9(2000), 700.
[16] ASTM E2283− 08, 2013.
[17] H.V. Atkinson, G. Shi: Prog. Mater. Sci., 48(2003), 457.
[18] ASTM E 45 – 05, 2002.
[19] Y. Murakami, S. Kodama, S. Konuma: Int. J. Fatigue., 11 (1989), 291.
[20] Y. Murakami, J. Res. NIST, 99 (1994), 345.
[21] S. Zhou, Y. Murakami, S. Beretta, Y. Fukushima: Mater. Sci. Tech., 18 (2002), 1535.
[22] Y. Murakami: Metal fatigue: effects of small defects and nonmetallic inclusions, Elsevier, Amsterdam & Boston, (2002).
[23] Y. Murakami, H. Matsunaga, A. Abyazi, Y. Fukushima: Fatigue Fract. Eng. Mater. Struct., 36(2013), 836.
[24] A. Roiko, H. Hänninen, H. Vuorikari: Int. J. fatigue, 41(2012), 158.
[25] Y. Murakami, T. Endo: Int. J. Fatigue, 2(1980), 23.
[26] J. Ekengren, J. Bergström: Extremes, 15(2012), 257.
[27] Y. Murakami, S. Beretta: Extremes, 2(1999), 123.
[28] A. Abyazi, M.S.c Thesis, Sahand University of Technology, 1387, in Persian.
[29] A. R. Ebrahimi, A. Abyazi, S. M. Abbasi: Int. J. ISSI, 5(2008), 14.
[30] A. R. Ebrahimi, A. Abyazi: 5th Middle East NDT Conference, Kingdom of Bahrain, (2009).
[31] A. Abyazi, A. R. Ebrahimi: The 2nd Int. conf. on Technical Inspection and NDT, Tehran, (2008), in Persian.
[32] A. R. Ebrahimi, H. Ebrahimpoor, A. Abyazi: Proc. of 11th steel symp., Shahid Chamran University, Ahvaz, Iran, (1387), 287, in Persian.
[33] A. Abyazi, H. Ebrahimpoor, A. R. Ebrahimi: The 2nd Joint Conf. of 12th Iranian Metall. Eng. Soc. Annual Cong. and 20th Iranian Foundry Society Seminar, Karaj, (2008), in Persian.
[34] A. R. Ebrahimi, A. Abyazi: The 2nd Int. conf. on Technical Inspection and NDT, Tehran, (2008), in Persian.
[35] S. Ganesh, R. D. Stout: Weld. J., (1976), 341-s.
[36] R. P. Oates, R. D. Stout, Weld. J. (1973), 481-s.
[37] C. Temmel, B. Karlsson, N. G. Ingesten: Metall. Mater. Trans. A, 37A(2006), 2995.
[38] K. Easterling, Introduction to the physical metallurgy of welding, Butterworths, London, (1992).
[39] Jan Mayén, S. A. Serna, B. Campillo, O. Flores: Mater. Sci. Eng. A, 582(2013), 22.
[40] A. Navarro, E. R. Delorios, Fatigue Eng. Mater. Struct., 11(1988), 383.
[41] J. L. Breat, F. Mudry, A. Pineau, Fatigue Eng. Mater. Struct., 6(1983), 349.
[42] N. Narasaiah, K.K. Ray: Mat. Sci. Eng. A, 474(2008), 48.
[43] N. Narasaiah, K. K. Ray, Mat. Sci. Eng. A, 392(2005), 269.
[44] K. Hussain, E. R. Delosrios, A. Navarro: Fatigue Eng. Mat. Struc., 44(1993), 425.
[45] Y. Kanbe, A. Karasev, H. Todoroki, P. G. Jonsso: steel res. Int., vol. 82(2011), 313.